

Quantum extraordinary-log universality of boundary critical behavior

Yanan Sun¹ and Jian-Ping Lv^{1,*}

¹*Department of Physics and Anhui Key Laboratory of Optoelectric Materials Science and Technology,
Key Laboratory of Functional Molecular Solids, Ministry of Education,
Anhui Normal University, Wuhu, Anhui 241000, China*

(Dated: December 6, 2022)

The recent discovery of extraordinary-log universality has generated intense interest in classical and quantum boundary critical phenomena. Despite tremendous efforts, the existence of quantum extraordinary-log universality remains extremely controversial. Here, by utilizing quantum Monte Carlo simulations, we study the quantum edge criticality of a two-dimensional Bose-Hubbard model featuring emergent bulk criticality. On top of an insulating bulk, the open edges experience a Kosterlitz-Thouless-like transition into the superfluid phase when the hopping strength is sufficiently enhanced on edges. At the bulk critical point, the open edges exhibit the special, ordinary, and extraordinary critical phases. In the extraordinary phase, logarithms are involved in the finite-size scaling of two-point correlation and superfluid stiffness, which admit a classical-quantum correspondence for the extraordinary-log universality. Thanks to modern quantum emulators for interacting bosons in lattices, the edge critical phases might be realized in experiments.

I. INTRODUCTION

Scaling and universality are pillars of modern critical phenomena [1]. In the paradigm of criticality, the two-point correlation $g(r)$ decays as the power law [1–4]

$$g(r) \sim r^{2-(d+z)-\eta} \quad (1)$$

with the spatial distance r , where d , z and η are respectively spatial dimension, dynamic critical exponent and anomalous dimension.

Boundary critical behavior (BCB) refers to the critical phenomena occurring on boundaries of a critical bulk [5–16] and relates to a rich variety of state-of-the-art concepts [17–23]. Recently, in the context of BCB, the extraordinary-log universality (ELU) was predicted by Metlitski for the classical three-dimensional (3D) $O(N)$ model with $2 \leq N < N_c$, where N_c is an upper bound [24]. For ELU the boundary two-point correlation $g(r)$ decays logarithmically with r as [24]

$$g(r) \sim [\ln(r)]^{-\hat{\eta}}, \quad (2)$$

where $\hat{\eta}$ is only dependent on N . Shortly afterwards, much attention was devoted to the BCB in classical [25–31] and quantum [32–36] systems.

Evidence for *classical* ELU was obtained from the Monte Carlo simulations of Heisenberg and XY models [25, 26, 28]. Inspired by the studies using magnetic fluctuations at different Fourier modes to explore precise finite-size scaling (FSS) [37, 38] as well as the two-length scenarios for high-dimensional Ising models [39–44] and deconfined criticality [45], an alternative scaling formula of $g(r)$ was conjectured for ELU [26]. This conjecture was based on the fact that the critical magnetic fluctuations at zero and smallest non-zero modes scale as $L^2[\ln(L)]^{-\hat{q}}$ and $L^2[\ln(L)]^{-\hat{\eta}}$, with the critical exponents \hat{q} and $\hat{\eta} = \hat{q} + 1$, respectively. This observation

can be related to the FSS of $g(r)$ as [26]

$$g(r) \sim \begin{cases} [\ln(r)]^{-\hat{\eta}}, & \ln(r) \leq \mathcal{O}[(\ln(L))^{\hat{q}/\hat{\eta}}], \\ [\ln(L)]^{-\hat{q}}, & \ln(r) \geq \mathcal{O}[(\ln(L))^{\hat{q}/\hat{\eta}}]. \end{cases} \quad (3)$$

With the concept “unwrapping” [40, 46, 47], a geometric explanation of two-length scenario was introduced based on unwrapped correlation length [40, 44, 48]. The two exponents \hat{q} and $\hat{\eta}$ were also observed in the classical ELU at an emergent $O(2)$ critical point [30]. Eq. (3) *formally* agrees with (2) on the FSS of $g(r)$ in the $r \rightarrow \infty$ limit.

Quantum edge criticality (QEC) has been extensively studied in the two-dimensional dimerized antiferromagnetic quantum (2D-DAQ) Heisenberg and XXZ models, which are prototype models for $O(3)$ and $O(2)$ criticality [13–16, 32–34], respectively. On one hand, the dangling edges of 2D-DAQ spin-1/2 and spin-1 Heisenberg models harbor the non-ordinary criticality [14–16, 32], where the critical exponents in magnetic sector are almost compatible with $O(3)$ special transition [14, 15]. The numerical results for scaling dimension Δ_n (Δ_v) of Néel (valence bond solid) order were compared [32] to the field-theoretic prediction [49]

$$\Delta_n - 1/2 = \epsilon_n \quad \text{and} \quad \Delta_v - 1/2 = -3\epsilon_n \quad (4)$$

with $\Delta_\phi - 3/2 = -\epsilon_n$, where $\Delta_\phi \approx 1.187$ [10] is the scaling dimension of spin order in $O(3)$ ordinary universality. For the spin-1/2 case, the results do not agree with Eq. (4) but conform with the scaling relation $3\Delta_n + \Delta_v = 2$. For the spin-1 case, the estimate $\Delta_v \approx -2$ is roughly compatible with the theory of extraordinary-power phase [24], hence in sharp contrast to Eq. (4) and the theory of ELU. On the other hand, the non-dangling edges of 2D-DAQ spin-1/2 Heisenberg model host the ordinary phase, special transition and *long-range ordered* extraordinary phase [14, 15, 33]. Moreover, the 2D-DAQ spin-1 XXZ model may exhibit the extraordinary-log criticality, yet this observation does not hold for the spin-1/2 case [34].

Hence, despite the tremendous efforts devoted to the BCB of quantum antiferromagnets, the existence of quantum ELU

* jplv2014@ahnu.edu.cn

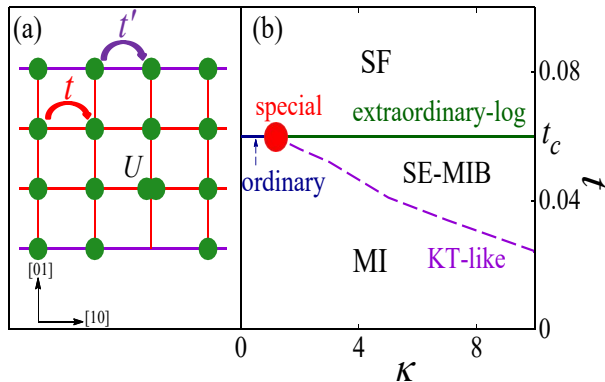


Figure 1. Model and ground-state phase diagram. (a) Definition of open-edge Bose-Hubbard model, where t and t' are hopping amplitudes and U denotes onsite repulsion. (b) The phase diagram in terms of t and the edge hopping enhancement κ , including a phase with superfluid edges and Mott insulating bulk (SE-MIB) as well as the phases of bulk-edge superfluid (SF) and Mott insulator (MI). These phases are separated by the Kosterlitz-Thouless-like (KT-like), extraordinary-log and ordinary critical lines that are terminated at the multi-critical special transition point.

remains extremely controversial. Moreover, as indicated in Ref. [24], the existing results can not form a self-contained picture for the classical-quantum correspondence of BCB and failed to realize quantum ELU. Here, we switch to interacting bosons and show that the open-edge Bose-Hubbard model hosts quantum ELU. This conclusion is based on the logarithmic FSS of two-point correlation and superfluid stiffness for extraordinary phase as well as an overall classical-quantum correspondence for various critical phases. The sharp difference from the BCB of XXZ antiferromagnet [34] reflects the sensitivity of BCB to geometric settings and local operators.

In the following, we focus on the open-edge Bose-Hubbard model and explore the quantum $O(2)$ BCB of the model. Section II defines the open-edge Bose-Hubbard model and presents its ground-state phase diagram. Section III introduces the methodology adopted throughout present study. Section IV presents Monte Carlo data and scaling analyses. A summary is finally given in Sec. V.

II. MODEL AND GROUND-STATE PHASE DIAGRAM

We consider the square-lattice Bose-Hubbard model at unit boson filling with the Hamiltonian

$$\hat{H} = - \sum_{\langle ij \rangle} t_{ij} (\hat{b}_i^\dagger \hat{b}_j + \hat{b}_j^\dagger \hat{b}_i) + \frac{U}{2} \sum_i \hat{n}_i (\hat{n}_i - 1), \quad (5)$$

where \hat{b}_i^\dagger and \hat{b}_i are respectively bosonic creation and annihilation operators at site i , and $\hat{n}_i = \hat{b}_i^\dagger \hat{b}_i$. t_{ij} denotes the amplitude of the nearest-neighbor hopping between i and j , and $U > 0$ represents onsite repulsion. The first summation

Table I. Leading scaling behaviors of the edge two-point correlation $g(L/2)$ and the superfluid stiffness ρ_s in critical phases.

Critical phase	$g(L/2)$	ρ_s
special	$L^{-\eta}$, $\eta \approx 0.65$	L^{-1}
KT-like	$L^{-\eta}$, $\eta = 1/4$	L^{-1}
SE-MIB	$L^{-\eta}$, $\eta \in (0, 1/4)$	L^{-1}
ordinary	$L^{-\eta}$, $\eta \approx 2.438$	L^{-1}
extraordinary	$[\ln(L)]^{-\hat{q}}$, $\hat{q} \approx 0.59$	$L^{-1} \ln(L)$

runs over pairs of nearest neighboring sites while the second summation is over sites. We set $U = 1$ as energy unit.

As illustrated by Fig. 1(a), we define our model for BCB by setting open and periodic boundary conditions along [01] and [10] directions, respectively. Hence, a pair of open edges are specified. The hopping amplitude $t_{ij} = t'$ on open edges is distinguished from $t_{ij} = t$ in bulk. The edge hopping enhancement is parameterized by $\kappa = (t' - t)/t$.

At $\kappa = 0$, model (5) reduces to the standard Bose-Hubbard model at unit boson filling [50], which has an *emergent* $O(2)$ quantum critical point separating the Mott insulating and superfluid phases. This critical point features Lorentz invariance with $z = 1$. The present authors and coworkers have given an estimate for the quantum critical point as $t_c = 0.0597291(8)$ [51], which agrees with the literature result $t_c = 0.05974(3)$ [52].

We explore quantum phases of model (5) by FSS and the results are summarized as a ground-state phase diagram in Fig. 1(b). There is a phase, dubbed SE-MIB, that features superfluid edges on top of Mott insulating bulk. Moreover, there are three critical edge phases at t_c : the ordinary, special and extraordinary-log phases. Scaling behaviors of edge critical phases are described in Table I [53].

III. METHODOLOGY

We apply the Prokof'ev-Svistunov-Tupitsyn worm quantum Monte Carlo algorithm [54, 55] to simulate model (5) in the imaginary-time path integral representation. The maximum side length of the square lattice is up to $L = 192$. The inverse temperature is set as $\beta = L$, which is in line with $z = 1$. We study the special, ordinary and extraordinary phases at $t_c = 0.0597291$ by varying κ , and explore the KT-like transition for $t < t_c$. In particular, we analyze the extraordinary phase in a broad parameter regime.

Analyses of the FSS involving $\ln(L)$ may be “notoriously difficult” [56]. We perform the analyses using least-squares fits. Following standard criterion, we prefer the fits with $\chi^2/DF \sim 1$, where χ^2 is the Chi squared and DF denotes the degree of freedom. We also examine the stability against varying L_{\min} , which represents the minimum side length involved in fitting.

IV. RESULTS

A. Special transition

We detect the special transition by tuning κ at $t = t_c$. We sample the winding probability $R_{[10]} = \langle \mathcal{R}_{[10]} \rangle$, where $\mathcal{R}_{[10]} = 1$ if there exists at least a particle line winding around the periodic [10] direction of square lattice. The winding probability is dimensionless and obeys the FSS $R_{[10]} = \tilde{R}_{[10]}(\epsilon L^{y_t})$, where $\epsilon = \kappa - \kappa_c$ represents the deviation from the critical point κ_c , and y_t relates to the correlation length exponent ν by $y_t = 1/\nu$. $R_{[10]}$ is useful for locating critical points [51]. Expanding $\tilde{R}_{[10]}$ and incorporating corrections to scaling, we obtain

$$R_{[10]} = R_{[10]}^c + \sum_j a_j \epsilon^j L^{j y_t} + \sum_m b_m L^{-\omega_m}, \quad (6)$$

where $R_{[10]}^c$ is somewhat universal, a_j ($j = 1, 2, \dots$) and b_m ($m = 1, 2, \dots$) are non-universal, and ω_m represents exponents for corrections. We show $R_{[10]}$ versus κ in Fig. 2(a), where a scaling invariance point is nearly at $\kappa \approx 1.2$. We fit $R_{[10]}$ data with $L = 48, 64, 96, 128$ and 192 to Eq. (6). We observe $\omega_1 \approx 1.4$, which is larger than $\omega_1 \approx 0.789$ of 3D O(2) value [57] and $\omega_1 = 1$ from boundary irrelevant fields [25]. The correction with $\omega_1 \leq 1$ is either absent or weak. Hence, we also perform fits without correction term and monitor the effects of corrections by examining the stability of fits upon gradually increasing L_{\min} . We obtain $\kappa_c = 1.206(7)$ and $y_t = 0.44(8)$ with $\chi^2/\text{DF} \approx 4.6$ for $L_{\min} = 64$, $\kappa_c = 1.184(6)$ and $y_t = 0.4(1)$ with $\chi^2/\text{DF} \approx 0.9$ for $L_{\min} = 96$, as well as $\kappa_c = 1.175(5)$ and $y_t = 0.8(3)$ with $\chi^2/\text{DF} \approx 0.2$ for $L_{\min} = 128$. Next, by fixing y_t at the estimate $y_t = 0.608$ for the special transition of classical O(2) model [10], we obtain $\kappa_c = 1.197(2)$, $1.180(3)$ and $1.175(7)$ with $\chi^2/\text{DF} \approx 4.6$, 1.1 and 0.3 , for $L_{\min} = 64, 96$ and 128 , respectively. When $y_t = 0.58$ is fixed, we obtain close estimates, which are detailed in Appendix C. By comparing all these fits, we finally estimate $\kappa_c = 1.18(2)$. For illustrating the single-variable function $\tilde{R}_{[10]}$ together with the estimates of κ_c and y_t , we plot $R_{[10]}$ versus ϵL^{y_t} in Fig. 2(a) with $\kappa_c = 1.18$ and $y_t = 0.608$, where finite-size corrections are already negligible for large systems.

Further evidence comes from the FSS of the superfluid stiffness ρ_s , which is defined as [58] $\rho_s = \langle \mathcal{W}_{[10]}^2 \rangle / (2t'\beta)$ through the fluctuations of the winding number $\mathcal{W}_{[10]}$ along the [10] direction of square lattice. At κ_c , ρ_s should scale as $\rho_s \sim L^{2-(d+z)}$. This scaling behavior is verified by Fig. 2(b) with $d = 2$ and $z = 1$: as $L \rightarrow \infty$, $\rho_s L$ is asymptotically a constant for $\kappa \leq \kappa_c$, but bends upwards for $\kappa > \kappa_c$.

We consider the two-point correlation $g(L/2)$ at the largest distance $r_{[10]} = L/2$ along an open edge, which is estimated from the random walks of the two defects in worm quantum Monte Carlo simulations. More descriptions and benchmarks for this estimator are presented in Appendix B. Figure 2(c) shows that the result at κ_c is compatible with the critical scaling behavior $g(L/2) \sim L^{-0.65}$, yet deviates when $\kappa \neq \kappa_c$.

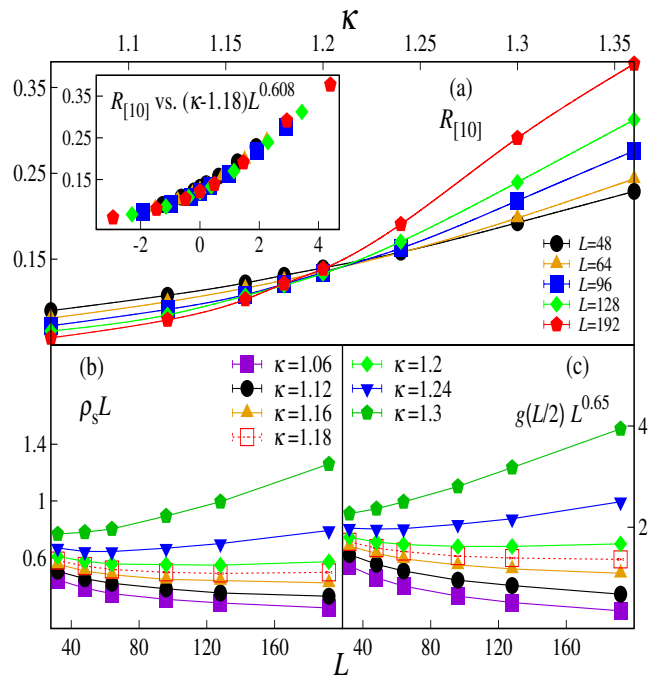


Figure 2. Special transition. (a) Winding probability $R_{[10]}$ versus κ . The inset displays $R_{[10]}$ versus $(\kappa - \kappa_c)L^{y_t}$ with $\kappa_c = 1.18$ and $y_t = 0.608$. (b) Scaled superfluid stiffness $\rho_s L$ versus L . (c) Scaled two-point correlation $g(L/2)L^{4-2y_h}$ with $y_h = 1.675$.

The scaling behavior at κ_c is accounted for by the O(2) special universality with the exponent $y_h \approx 1.675$ [10, 30, 31, 59], as $g(L/2) \sim L^{2y_h-4}$.

B. KT-like criticality

Figure 3(a) shows $R_{[10]}$ versus t for $\kappa = 10$. Around $t_x \approx 0.023$, $R_{[10]}$ varies drastically. For $t > t_x$, $R_{[10]}$ extrapolates to a nontrivial value in the $L \rightarrow \infty$ limit, which is dependent on t . Meanwhile, the superfluid stiffness scales as $\rho_s \sim L^{-1}$. These observations indicate a regime of critical phase.

The KT-like criticality is evidenced by the anomalous dimension η . Figure 3(b) demonstrates that, at $t_{\text{KT}} \approx t_x$, $g(L/2)$ scales as $g(L/2) \sim L^{2-(d+z)-\eta}$ with $d = 1$, $z = 1$ and $\eta = 1/4$. The value $1/4$ is consistent with that of the KT transition in 2D XY model [60]. For $t > t_{\text{KT}}$, we fit $g(L/2)$ to the formula $g(L/2) \sim L^{-\eta}$ of leading scaling. The fits are illustrated by Fig. 3(c) and detailed in Appendix C. In particular, for $t = 0.027$ and 0.05 , we obtain $\eta = 0.150(2)$ and $0.058(4)$ respectively, with $\chi^2/\text{DF} \approx 1.0$ and $L_{\min} = 96$. The continuously varying exponent η is reminiscent of the low-temperature critical phase of 2D XY model [61].

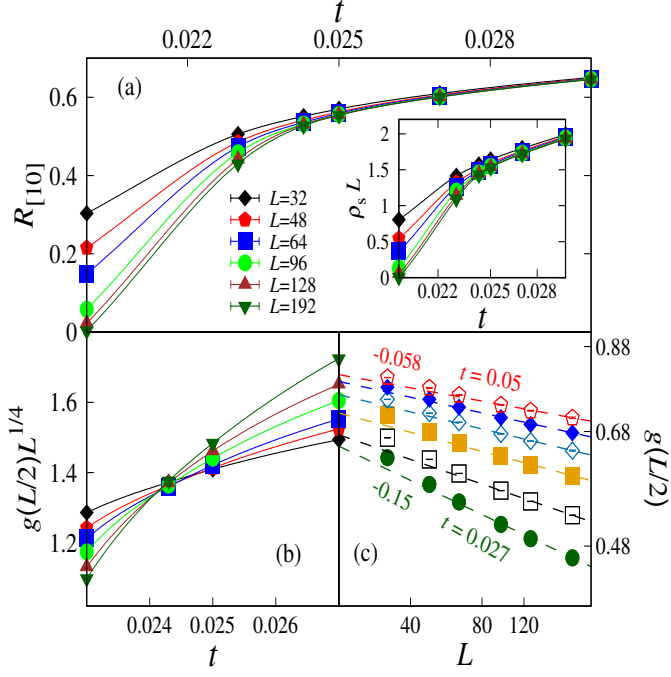


Figure 3. KT-like criticality ($\kappa = 10$). (a) Winding probability $R_{[10]}$ versus t . The inset displays the scaled superfluid stiffness $\rho_s L$. (b) Scaled two-point correlation $g(L/2)L^{1/4}$ versus t . (c) Log-log plot of $g(L/2)$ versus L .

C. Ordinary critical phase

Corresponding to classical O(2) BCB, the small- κ side of special transition may fall into the ordinary critical universality class. For $\kappa = 0.4$, Fig. 4 demonstrates that $g(L/2)$ scales as $L^{2-(d+z)-\eta}$ with $\eta \approx 2.438$, $d = 1$ and $z = 1$. The value of η relates to $y_h = 0.781(2)$ [10] of the O(2) BCB by $\eta = 4 - 2y_h$. As $L \rightarrow \infty$, $\rho_s L$ and $R_{[10]}$ tend to be independent of L . These scaling behaviors indicate the existence of the O(2) quantum ordinary universality.

D. Extraordinary-log critical phase

To explore the extraordinary phase, we make use of a broad parameter regime in the large- κ side of special transition. In the ELU, $g(L/2)$ scales as [24]

$$g(L/2) = a[\ln(L/l_0)]^{-\hat{q}}, \quad (7)$$

where l_0 is a reference length and a denotes a non-universal constant. For the classical XY model, this scaling form was verified and $\hat{q} = 0.59(2)$ was estimated [26]. Close values of \hat{q} were obtained for the classical ELU of O(2) model [28] and emergent O(2) criticality [30, 31]. We perform fits for $g(L/2)$ according to Eq. (7) and obtain $0.3 \lesssim \hat{q} \lesssim 0.7$ for $\kappa = 2, 3, 5$ and 7 . We observe that l_0 decreases significantly as κ increases. These features conform to the observations for classical ELU in Ref. [26]. When $\hat{q} = 0.59$ is fixed, we achieve,

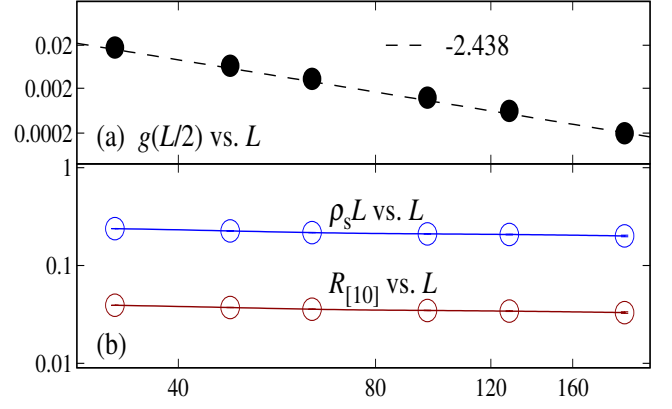


Figure 4. Ordinary critical phase ($\kappa = 0.4$). (a) Log-log plot of two-point correlation $g(L/2)$ versus L . The slope -2.438 relates to $2y_h - 4$ with $y_h = 0.781$. (b) Log-log plot of scaled superfluid stiffness $\rho_s L$ and winding probability $R_{[10]}$ versus L .

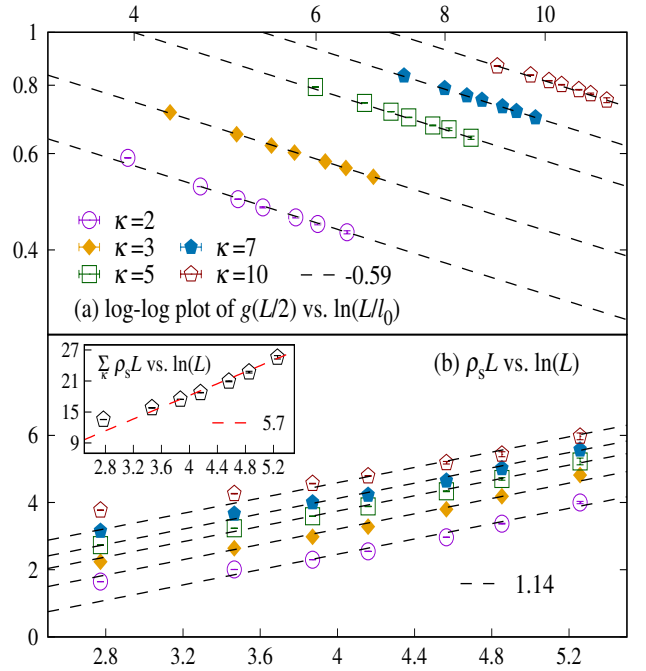


Figure 5. Extraordinary-log critical phase. (a) Log-log plot of two-point correlation $g(L/2)$ versus $\ln(L/l_0)$, where the values of l_0 come from preferred fits. The slope -0.59 relates to $-\hat{q}$. (b) Scaled superfluid stiffness $\rho_s L$ versus $\ln(L)$. Inset: the summation of $\rho_s L$ over κ . The slopes 1.14 and 5.7 denote b in Eq. (8) and $5b$, respectively.

for each κ , stable fitting results for l_0 and a . Instance results of l_0 include $l_0 = 0.31(3), 0.21(1), 0.04(4), 0.0108(5)$ and $0.002(1)$ with $\chi^2/DF \approx 0.3, 1.8, 0.9, 0.7$ and 0.5 , for $\kappa = 2, 3, 5, 7$ and 10 , respectively. The power-law dependence of $g(L/2)$ on $\ln(L/l_0)$ is illustrated by Fig. 5(a).

From Fig. 5(b), we find that $\rho_s L$ roughly obeys the loga-

rithmic scaling formula

$$\rho_s L = b \ln(L) + c \quad (8)$$

with universal $b \approx 1.1$ and non-universal c . Preferred fits are achieved in deep extraordinary regime. With $L_{\max} = 192$, we obtain $b = 1.14(3)$, $1.15(3)$ and $1.1(1)$ with $\chi^2/\text{DF} \approx 0.9$, 2.8 and 0.7 , for $\kappa = 5, 7$ and 10 , respectively. We also perform fits to $\sum_{\kappa} \rho_s L = 5b \ln(L) + C$ (C is a fitting parameter) where the summation runs over the set $\{2, 3, 5, 7, 10\}$ of κ . For $L_{\min} = 64$, we obtain reasonably good results as $5b = 5.8(2)$ and $C = -5.3(7)$ with $\chi^2/\text{DF} \approx 2.0$ and $L_{\max} = 192$, as well as $5b = 5.6(2)$ and $C = -4.6(8)$ with $\chi^2/\text{DF} \approx 0.8$ and $L_{\max} = 128$. These fits are consistent and finally yield $5b = 5.7(3)$, which relates to $b = 1.14(6)$. By contrast, the logarithmic divergence of $\rho_s L$ is absent in the paradigm of criticality, as illustrated for special transition [Fig. 2(b)] and ordinary critical phase [Fig. 4(b)], and does not emerge in the KT-like criticality [Fig. 3(a)]. The logarithmic FSS (8) with unit exponent and universal coefficient resembles that of the helicity modulus in classical XY and Heisenberg models [24–26].

V. SUMMARY

The extensive ongoing activities in the search for quantum ELU are restricted to dimerized antiferromagnets, for which

conclusive evidence remains unavailable. Here, we switch to interacting bosons by formulating an open-edge Bose-Hubbard model and demonstrate the emergence of quantum ELU. An edge superfluid phase is observed on top of an insulating bulk. When the bulk is at the emergent quantum critical point, the special, ordinary and extraordinary-log critical phases emerge on open edges. In the extraordinary-log critical phase, the leading FSS for the largest-distance two-point correlation and scaled superfluid stiffness are logarithmic. By an overall classical-quantum correspondence of $O(2)$ BCB as well as the universal behavior of logarithmic FSS in the extraordinary phase, we provide complementary evidence for the existence of quantum ELU. As the Bose-Hubbard model can be accessed by quantum emulators with ultracold bosons in optical lattices [62–65], our results indicate a possible experimental scheme for realizing ELU.

ACKNOWLEDGMENTS

One of us (J.P.L.) wishes to warmly thank Youjin Deng for the collaboration in earlier related studies. The present work has been supported by the National Natural Science Foundation of China (under Grant Nos. 12275002, 11975024, and 11774002) and the Education Department of Anhui.

-
- [1] H. E. Stanley, “Scaling, universality, and renormalization: Three pillars of modern critical phenomena,” *Rev. Mod. Phys.* **71**, S358 (1999).
 - [2] C. Domb, *The critical point: a historical introduction to the modern theory of critical phenomena* (CRC Press, 1996).
 - [3] S. Sachdev, *Quantum phase transitions* (Wiley Online Library, 2007).
 - [4] R. Fernández, J. Fröhlich, and A. D. Sokal, *Random walks, critical phenomena, and triviality in quantum field theory* (Springer, Berlin, 2013).
 - [5] K. Binder and P. C. Hohenberg, “Surface effects on magnetic phase transitions,” *Phys. Rev. B* **9**, 2194 (1974).
 - [6] K. Ohno and Y. Okabe, “The $1/n$ expansion for the extraordinary transition of semi-infinite system,” *Prog. Theor. Phys.* **72**, 736–745 (1984).
 - [7] D. P. Landau, R. Pandey, and K. Binder, “Monte carlo study of surface critical behavior in the xy model,” *Phys. Rev. B* **39**, 12302 (1989).
 - [8] H. W. Diehl, “The theory of boundary critical phenomena,” *Int. J. Mod. Phys. B* **11**, 3503–3523 (1997), arXiv:cond-mat/9610143 [cond-mat].
 - [9] M. Pleimling, “Critical phenomena at perfect and non-perfect surfaces,” *J. Phys. A: Math. and Gen.* **37**, R79 (2004), arXiv:cond-mat/0402574 [cond-mat].
 - [10] Y. Deng, H. W. J. Blöte, and M. P. Nightingale, “Surface and bulk transitions in three-dimensional $o(n)$ models,” *Phys. Rev. E* **72**, 016128 (2005), arXiv:cond-mat/0504173 [cond-mat].
 - [11] Y. Deng, “Bulk and surface phase transitions in the three-dimensional $o(4)$ spin model,” *Phys. Rev. E* **73**, 056116 (2006).
 - [12] J. Dubail, J. L. Jacobsen, and H. Saleur, “Exact solution of the anisotropic special transition in the $o(n)$ model in two dimensions,” *Phys. Rev. Lett.* **103**, 145701 (2009), arXiv:0909.2949 [cond-mat].
 - [13] L. Zhang and F. Wang, “Unconventional surface critical behavior induced by a quantum phase transition from the two-dimensional affleck-kennedy-lieb-tasaki phase to a néel-ordered phase,” *Phys. Rev. Lett.* **118**, 087201 (2017), arXiv:1611.06477 [cond-mat].
 - [14] C. Ding, L. Zhang, and W. Guo, “Engineering surface critical behavior of $(2+1)$ -dimensional $o(3)$ quantum critical points,” *Phys. Rev. Lett.* **120**, 235701 (2018), arXiv:1801.10035 [cond-mat].
 - [15] L. Weber, F. Parisen Toldin, and S. Wessel, “Nonordinary edge criticality of two-dimensional quantum critical magnets,” *Phys. Rev. B* **98**, 140403(R) (2018), arXiv:1804.06820 [cond-mat].
 - [16] L. Weber and S. Wessel, “Nonordinary criticality at the edges of planar spin-1 heisenberg antiferromagnets,” *Phys. Rev. B* **100**, 054437 (2019), arXiv:1906.07051 [cond-mat].
 - [17] J. Cardy, “Boundary conformal field theory,” arXiv:hep-th/0411189 [cond-mat].
 - [18] T. Grover and A. Vishwanath, “Quantum criticality in topological insulators and superconductors: Emergence of strongly coupled majoranas and supersymmetry,” arXiv:1206.1332 [cond-mat].
 - [19] D. E. Parker, T. Scaffidi, and R. Vasseur, “Topological luttinger liquids from decorated domain walls,” *Phys. Rev. B* **97**, 165114 (2018), arXiv:1711.09106 [cond-mat].

- [20] D. Poland, S. Rychkov, and A. Vichi, “The conformal bootstrap: Theory, numerical techniques, and applications,” *Rev. Mod. Phys.* **91**, 015002 (2019), arXiv:1805.04405 [cond-mat].
- [21] S. Liu, H. Shapourian, A. Vishwanath, and M. A. Metlitski, “Magnetic impurities at quantum critical points: Large- n expansion and connections to symmetry-protected topological states,” *Phys. Rev. B* **104**, 104201 (2021), arXiv:2104.15026 [cond-mat].
- [22] D. M. Dantchev and S. Dietrich, “Critical casimir effect: Exact results,” arXiv:2203.15050 [cond-mat].
- [23] N. Andrei, A. Bissi, M. Buican, J. Cardy, P. Dorey, N. Drukker, J. Erdmenger, D. Friedan, D. Fursaev, A. Konechny, C. Kristjansen, I. Makabe, Y. Nakayama, A. O’Bannon, R. Parini, B. Robinson, S. Ryu, C. Schmidt-Colinet, V. Schomerus, C. Schweigert, and G. M. T. Watts, “Boundary and defect CFT: open problems and applications,” *J. Phys. A: Math. and Theo.* **53**, 453002 (2020), arXiv:1810.05697 [cond-mat].
- [24] M. A. Metlitski, “Boundary criticality of the $o(n)$ model in $d=3$ critically revisited,” *SciPost Phys.* **12**, 131 (2022), arXiv:2009.05119 [cond-mat].
- [25] F. Parisen Toldin, “Boundary critical behavior of the three-dimensional heisenberg universality class,” *Phys. Rev. Lett.* **126**, 135701 (2021), arXiv:2012.00039 [cond-mat].
- [26] M. Hu, Y. Deng, and J.-P. Lv, “Extraordinary-log surface phase transition in the three-dimensional xy model,” *Phys. Rev. Lett.* **127**, 120603 (2021), arXiv:2104.05152 [cond-mat].
- [27] J. Padayasi, A. Krishnan, M. A. Metlitski, I. A. Gruzberg, and M. Meineri, “The extraordinary boundary transition in the 3d $o(n)$ model via conformal bootstrap,” *SciPost Phys.* **12**, 190 (2022), arXiv:2111.03071 [cond-mat].
- [28] F. Parisen Toldin and M. A. Metlitski, “Boundary criticality of the 3d $o(n)$ model: From normal to extraordinary,” *Phys. Rev. Lett.* **128**, 215701 (2022), arXiv:2111.03613 [cond-mat].
- [29] F. Parisen Toldin, “Surface critical behavior of the three-dimensional $o(3)$ model,” *J. Phys.: Conf. Ser.* **2207**, 012003 (2022), arXiv:2111.11762 [cond-mat].
- [30] L.-R. Zhang, C. Ding, Y. Deng, and L. Zhang, “Surface criticality of the antiferromagnetic potts model,” *Phys. Rev. B* **105**, 224415 (2022), arXiv:2204.11692 [cond-mat].
- [31] X. Zou, S. Liu, and W. Guo, “Surface critical properties of the three-dimensional clock model,” *Phys. Rev. B* **106**, 064420 (2022), arXiv:2204.13612 [cond-mat].
- [32] L. Weber and S. Wessel, “Spin versus bond correlations along dangling edges of quantum critical magnets,” *Phys. Rev. B* **103**, L020406 (2021), arXiv:2010.15691 [cond-mat].
- [33] C. Ding, W. Zhu, W. Guo, and L. Zhang, “Special transition and extraordinary phase on the surface of a $(2+1)$ -dimensional quantum heisenberg antiferromagnet,” arXiv:2110.04762 [cond-mat].
- [34] W. Zhu, C. Ding, L. Zhang, and Guo W., “Exotic surface behaviors induced by geometrical settings of two-dimensional dimerized quantum xxz model,” arXiv:2111.12336 [cond-mat].
- [35] X.-J. Yu, R.-Z. Huang, H.-H. Song, L. Xu, C. Ding, and L. Zhang, “Conformal boundary conditions of symmetry-enriched quantum critical spin chains,” *Phys. Rev. Lett.* **129**, 210601 (2022), arXiv:2111.10945 [cond-mat].
- [36] Y. Xu, Z. Xiong, and L. Zhang, “Persistent corner spin mode at the quantum critical point of a plaquette heisenberg model,” arXiv:2112.04616 [cond-mat].
- [37] M. Wittmann and A. P. Young, “Finite-size scaling above the upper critical dimension,” *Phys. Rev. E* **90**, 062137 (2014), arXiv:1410.5296 [cond-mat].
- [38] E. Flores-Sola, B. Berche, R. Kenna, and M. Weigel, “Role of fourier modes in finite-size scaling above the upper critical dimension,” *Phys. Rev. Lett.* **116**, 115701 (2016), arXiv:1511.04321 [cond-mat].
- [39] V. Papanthakos, *Finite-size effects in high-dimensional statistical mechanical systems: The Ising model with periodic boundary conditions* (Ph.D. thesis, Princeton University, Princeton, New Jersey, 2006).
- [40] J. Grimm, E. M. Elçi, Z. Zhou, T. M. Garoni, and Y. Deng, “Geometric explanation of anomalous finite-size scaling in high dimensions,” *Phys. Rev. Lett.* **118**, 115701 (2017), arXiv:1612.01722 [cond-mat].
- [41] Z. Zhou, J. Grimm, S. Fang, Y. Deng, and T. M. Garoni, “Random-length random walks and finite-size scaling in high dimensions,” *Phys. Rev. Lett.* **121**, 185701 (2018), arXiv:1809.00515 [cond-mat].
- [42] S. Fang, J. Grimm, Z. Zhou, and Y. Deng, “Complete graph and gaussian fixed-point asymptotics in the five-dimensional fortuin-kasteleyn ising model with periodic boundaries,” *Phys. Rev. E* **102**, 022125 (2020), arXiv:1909.04328 [cond-mat].
- [43] J.-P. Lv, W. Xu, Y. Sun, K. Chen, and Y. Deng, “Finite-size scaling of $o(n)$ systems at the upper critical dimensionality,” *Natl. Sci. Rev.* **8**, nwaa212 (2021), arXiv:1909.10347 [cond-mat].
- [44] S. Fang, Y. Deng, and Z. Zhou, “Logarithmic finite-size scaling of the self-avoiding walk at four dimensions,” *Phys. Rev. E* **104**, 064108 (2021), arXiv:2103.04340 [cond-mat].
- [45] H. Shao, W. Guo, and A. W. Sandvik, “Quantum criticality with two length scales,” *Science* **352**, 213–216 (2016), arXiv:1603.02171 [cond-mat].
- [46] M. Heydenreich and R. Van der Hofstad, *Progress in high-dimensional percolation and random graphs* (Springer, 2017).
- [47] G. Bet, K. Bogerd, R. M. Castro, and R. van der Hofstad, “Detecting a botnet in a network,” *Math. Stat. Learn.* **3**, 315–343 (2021), arXiv:2005.10650 [cond-mat].
- [48] Y. Deng, T. M. Garoni, J. Grimm, and Z. Zhou, “Unwrapped two-point functions on high-dimensional tori,” *J. Stat. Mech.: Theo. and Exp.* **2022**, 053208 (2022), arXiv:2203.05100 [cond-mat].
- [49] C.-M. Jian, Y. Xu, X.-C. Wu, and C. Xu, “Continuous neel-vbs quantum phase transition in non-local one-dimensional systems with $so(3)$ symmetry,” *SciPost Physics* **10**, 033 (2021), arXiv:2004.07852 [cond-mat].
- [50] M. P. A. Fisher, P. B. Weichman, G. Grinstein, and D. S. Fisher, “Boson localization and the superfluid-insulator transition,” *Phys. Rev. B* **40**, 546–570 (1989).
- [51] W. Xu, Y. Sun, J.-P. Lv, and Y. Deng, “High-precision monte carlo study of several models in the three-dimensional $u(1)$ universality class,” *Phys. Rev. B* **100**, 064525 (2019), arXiv:1908.10990 [cond-mat].
- [52] B. Capogrosso-Sansone, Ş. G. Söyler, N. Prokof’ev, and B. Svistunov, “Monte carlo study of the two-dimensional bose-hubbard model,” *Phys. Rev. A* **77**, 015602 (2008), arXiv:0710.2703 [cond-mat].
- [53] Logarithmic corrections may emerge for the KT-like transition and the SE-MIB phase [61].
- [54] N. V. Prokof’ev, B. V. Svistunov, and I. S. Tupitsyn, “Exact, complete, and universal continuous-time worldline monte carlo approach to the statistics of discrete quantum systems,” *Sov. Phys. JETP* **87**, 310–321 (1998), arXiv:cond-mat/9703200 [cond-mat].
- [55] N. V. Prokof’ev, B. V. Svistunov, and I. S. Tupitsyn, ““worm” algorithm in quantum monte carlo simulations,” *Phys. Lett. A* **238**, 253–257 (1998).
- [56] P. Grassberger, “Critical percolation in high dimensions,” *Phys. Rev. E* **67**, 036101 (2003), arXiv:cond-mat/0202144 [cond-

- mat].
- [57] R. Guida and J. Zinn-Justin, “Critical exponents of the n -vector model,” *J. Phys. A: Math. Gen.* **31**, 8103 (1998), arXiv:cond-mat/9803240 [cond-mat].
- [58] E. L. Pollock and D. M. Ceperley, “Path-integral computation of superfluid densities,” *Phys. Rev. B* **36**, 8343–8352 (1987).
- [59] Y. Sun, J. Lyu, and J.-P. Lv, “Classical-quantum correspondence of special and extraordinary-log criticality: Villain’s bridge,” *Phys. Rev. B* **106**, 174516 (2022), arXiv:2211.11376 [cond-mat].
- [60] J. M. Kosterlitz, “The critical properties of the two-dimensional xy model,” *J. Phys. C: Solid State Phys.* **7**, 1046 (1974).
- [61] J. M. Kosterlitz, “Kosterlitz–thouless physics: a review of key issues,” *Rep. Prog. Phys.* **79**, 026001 (2016).
- [62] D. Jaksch, C. Bruder, J. I. Cirac, C. W. Gardiner, and P. Zoller, “Cold bosonic atoms in optical lattices,” *Phys. Rev. Lett.* **81**, 3108 (1998), arXiv:cond-mat/9805329 [cond-mat].
- [63] M. Greiner, O. Mandel, T. Esslinger, T. W. Hänsch, and I. Bloch, “Quantum phase transition from a superfluid to a mott insulator in a gas of ultracold atoms,” *Nature* **415**, 39–44 (2002).
- [64] S. Baier, M. J. Mark, D. Petter, K. Aikawa, L. Chomaz, Z. Cai, M. Baranov, P. Zoller, and F. Ferlaino, “Extended bose-hubbard models with ultracold magnetic atoms,” *Science* **352**, 201–205 (2016), arXiv:1507.03500 [cond-mat].
- [65] B. Yang, H. Sun, C.-J. Huang, H.-Y. Wang, Y. Deng, H.-N. Dai, Z.-S. Yuan, and J.-W. Pan, “Cooling and entangling ultracold atoms in optical lattices,” *Science* **369**, 550–553 (2020), arXiv:1901.01146 [cond-mat].
- [66] J. Salas, “Phase diagram for the bisected-hexagonal-lattice five-state potts antiferromagnet,” *Phys. Rev. E* **102**, 032124 (2020), arXiv:2006.04866 [cond-mat].
- [67] N. Prokof’ev and B. Svistunov, “Worm algorithms for classical statistical models,” *Phys. Rev. Lett.* **87**, 160601 (2001), arXiv:cond-mat/0103146 [cond-mat].

Appendix A: Details of methodology

In the appendixes, we present details for Monte Carlo simulations and provide a benchmark for two-point correlation using bulk criticality. We then analyze the data for the quantum critical phenomena on open edges, which include the special transition, the Kosterlitz-Thouless-like criticality, the ordinary critical phase and the extraordinary-log critical phase.

The raw data are all obtained from quantum Monte Carlo simulations, by means of the worm algorithm in the continuous-time path integral representation. The side lengths of square lattices include $L = 16, 32, 48, 64, 96, 128$ and 192 . In the worm simulations, the number of tentative updates for the defects, usually denoted by *Ira* (I) and *Masha* (M), ranges from 3.6×10^{12} to 3.4×10^{13} for $16 \leq L \leq 48$, and from 1.8×10^{13} to 3.7×10^{13} for $64 \leq L \leq 192$.

We perform FSS analyses by using least-squares fits. To this end, we utilize the function `NonlinearModelFit` in `Mathematica`, as adopted in Ref. [66]. According to standard criterion, we prefer the fits with $\chi^2/\text{DF} \sim 1$, where χ^2/DF represents the Chi squared per degree of freedom. We draw conclusions by comparing the fits that are stable against varying L_{\min} , which is the minimum side length incorporated in fitting. In certain situations, we also include a cutoff L_{\max} for

larger sizes.

Appendix B: Benchmark for two-point correlation using bulk criticality

We use an estimator of equal-imaginary-time correlations, which avoids reweighting along imaginary-time axis and turns out to be computationally cheap. The estimator correctly captures the asymptotic behavior in the $L \rightarrow \infty$ limit. Specifically speaking, in the worm quantum Monte Carlo simulations, we trace the trajectories of the defects I and M on an edge. If the imaginary-time distance between the defects is less than the $1/L$ fraction of entire axis, the distance r of two defects along the edge is recorded. The follow-up treatment is similar to the measurement of two-point correlations in a classical model [43] which was based on the original idea in Ref. [67]. We use the $r = 1$ result to normalize the two-point correlation and concentrate on the $r \neq 0$ domain of correlation function. Hence, the results do not suffer from the biased allocations of statistical weight between original and Green function state spaces. Finally, we obtain the two-point correlation $g(r)$ as a function of r along the edge.

We proceed to benchmark the above-mentioned methodology for correlation function using the bulk criticality. Particularly, we apply periodic conditions for both [10] and [01] directions to eliminate the open edges and sample the correlation functions at t_c . We analyze the r dependence of $g(r)$ as well as the L -dependent behavior of $g(L/2)$. We quote a precise estimate $\eta = 0.03853(48)$ for the anomalous dimension of the (2+1)-dimensional $O(2)$ criticality [51]. As shown in Fig. 6(a), the r -dependent behavior converges to the power law $g(r) \sim r^{2-(d+z)-\eta}$, with $d = 2$, $z = 1$ and $\eta \approx 0.03853$. From Fig. 6(b), we verify that $g(L/2)$ scales as $g(L/2) \sim L^{-1.03853}$.

More quantitative verification can be achieved by least-squares fits. We fit $g(L/2)$ to

$$g(L/2) = aL^b, \quad (\text{B1})$$

where a is a constant and $b = -1 - \eta$. The results are summarized in Table II. We obtain $b = -1.027(6)$ and $\chi^2/\text{DF} \approx 1.2$ for $L_{\min} = 48$, $b = -1.03(1)$ and $\chi^2/\text{DF} \approx 1.5$ for $L_{\min} = 64$, as well as $b = -1.06(3)$ and $\chi^2/\text{DF} \approx 1.4$ for $L_{\min} = 96$. The estimates of b are consistent with $-1 - \eta = -1.03853(48)$ of the (2+1)-dimensional $O(2)$ universality.

Appendix C: Details of the FSS analyses for BCB

In this appendix, we perform FSS analyses for the special transition, the Kosterlitz-Thouless-like criticality, the ordinary critical phase and the extraordinary-log critical phase.

Special transition. We locate the special transition point using the FSS of the winding probability $R_{[10]}$. We perform fits according to

$$R_{[10]} = R_{[10]}^c + a_1(\kappa - \kappa_c)L^{y_t} + b_1L^{-\omega_1}, \quad (\text{C1})$$

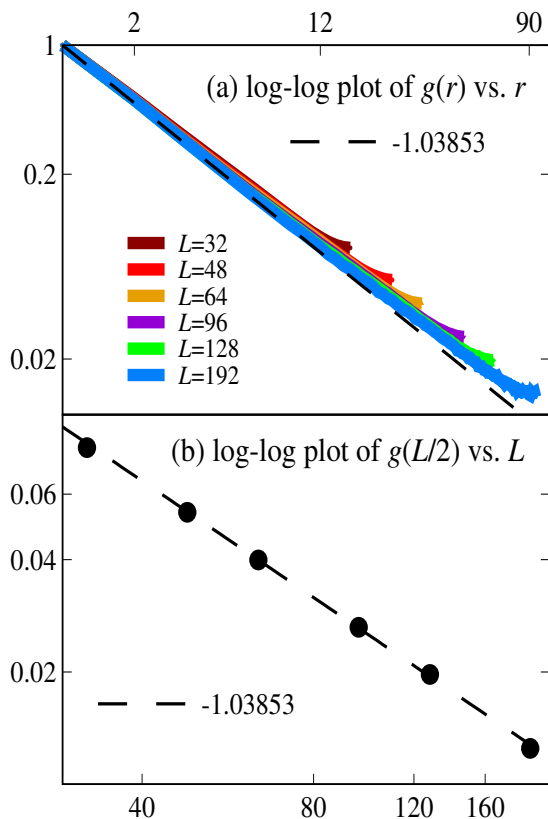


Figure 6. Bulk criticality. (a) Log-log plot of $g(r)$ versus r . (b) Log-log plot of $g(L/2)$ versus L .

Table II. Fits of $g(L/2)$ to Eq. (B1) at the bulk critical point.

L_{\min}	χ^2/DF	a	b
32	20.62/4	2.65(3)	-1.009(3)
48	3.45/3	2.86(6)	-1.027(6)
64	3.04/2	2.9(1)	-1.03(1)
96	1.41/1	3.4(4)	-1.06(3)

where $R_{[10]}^c$ is the critical dimensionless ratio, a_1 and b_1 represent fitting parameters, κ_c denotes the transition point, y_t relates to the correlation length exponent ν by $y_t = 1/\nu$, and ω_1 denotes the exponent for leading finite-size corrections. We perform least-squares fits with $\kappa = 1.16, 1.18, 1.2$ and $L = 48, 64, 96, 128, 192$. We consider the situations with y_t being free or fixed at 0.608 and 0.58, which were estimated for the special transition of classical O(2) model in spin [10] and flow [59] representations, respectively. For each situation, we obtain reasonably good results for large L_{\min} . When the leading correction term is present, the best estimate of ω_1 is $\omega_1 \approx 1.4$ (Table III), which is larger than $\omega_1 = 0.789$ of 3D O(2) value [57] and $\omega_1 = 1$ originating from boundary irrelevant fields [25], indicating that the correction term with $\omega_1 \leq 1$ is either absent or weak. Hence, as shown in Table IV, we also perform fits without incorporating correction

term, which have a reduced number of fitting parameters, and examine the stability of fitting results by varying L_{\min} . By comparing the fits, our final estimate of κ_c is $\kappa_c = 1.18(2)$.

Kosterlitz-Thouless-like critical phase. We explore the critical phase on the large- t side of Kosterlitz-Thouless-like transition for $\kappa = 10$. For each t in the set $\{0.027, 0.03, 0.035, 0.04, 0.045, 0.05\}$, we perform scaling analyses for $g(L/2)$ according to Eq. (B1) with $b = -\eta$, which corresponds to the leading FSS. The results are summarized in Table V, which demonstrates that the fits are precise only at large sizes. Moreover, as t increases, the exponent η decreases.

Ordinary critical phase. We analyze the ordinary critical phase at $\kappa = 0.4$ and $t = t_c$. We fit $g(L/2)$ to Eq. (B1) with $b = 2y_h - 4$. The results are presented in Table VI. For $L_{\min} = 48, 64$ and 96 , we find $b = -2.41(2), -2.45(4)$ and $-2.5(1)$ with $\chi^2/\text{DF} \approx 1.3, 1.1$ and 1.4 , respectively. These results are compatible with the exponent $2y_h - 4$ with $y_h = 0.781(2)$ of the classical O(2) ordinary surface criticality [10]. If a correction term is included and the fitting ansatz becomes $g(L/2) = L^b(a + cL^{-\omega_1})$, the effects from corrections decrease rapidly with L as $L^{b-\omega_1}$. It is practically difficult to estimate the amplitude of finite-size corrections.

Extraordinary critical phase. We analyze the FSS for the extraordinary phase. We fit $g(L/2)$ to

$$g(L/2) = a[\ln(L/l_0)]^{-\hat{q}}. \quad (\text{C2})$$

The results are given in Table VII. If \hat{q} is free, we obtain $0.3 \lesssim \hat{q} \lesssim 0.7$ and find that l_0 drastically decreases upon increasing κ . When $\hat{q} = 0.59$ is fixed, we obtain stable fitting results of a and l_0 for each considered κ . For l_0 , instance results are $l_0 = 0.31(3), 0.21(1), 0.04(4), 0.0108(5)$ and $0.002(1)$ with $\chi^2/\text{DF} \approx 0.3, 1.8, 0.9, 0.7$ and 0.5 , for $\kappa = 2, 3, 5, 7$ and 10 , respectively.

Assuming the existence of extraordinary-log critical universality, for each κ , we fit the data of ρ_s to

$$\rho_s L = a + b \ln L. \quad (\text{C3})$$

We obtain preferred fits with $L_{\max} = 192$ for the deep extraordinary regime. For $\kappa = 5$, we obtain $b = 1.14(3)$ with $L_{\min} = 64$ and $\chi^2/\text{DF} \approx 0.9$. For $\kappa = 7$, we obtain $b = 1.15(3)$ with $L_{\min} = 64$ and $\chi^2/\text{DF} \approx 2.8$. For $\kappa = 10$, we obtain $b = 1.1(1)$ with $L_{\min} = 96$ and $\chi^2/\text{DF} \approx 0.7$. To obtain a unique estimate of fitting parameters, we analyze the sum of the scaled superfluid stiffness $\rho_s L$ over $\kappa = 2, 3, 5, 7$ and 10 by performing fits to

$$\sum_{\kappa} \rho_s L = A + B \ln L. \quad (\text{C4})$$

As summarized in Table VIII, we obtain reasonably good fits with $\chi^2/\text{DF} \sim 1$ for $L_{\max} = 192$ and 128 . For $L_{\max} = 192$, we obtain $A = -5.3(7)$, $B = 5.8(2)$ and $\chi^2/\text{DF} \approx 2.0$ with $L_{\min} = 64$, as well as $A = -8.8(2.0)$, $B = 6.5(4)$ and $\chi^2/\text{DF} \approx 0.5$ with $L_{\min} = 96$. For $L_{\max} = 128$, we obtain $A = -4.6(8)$, $B = 5.6(2)$ and $\chi^2/\text{DF} \approx 0.8$ with $L_{\min} = 64$.

Table III. Fits of $R_{[10]}$ to Eq. (C1) for the special transition.

L_{\min}	χ^2/DF	κ_c	y_t	$R_{[10]}^c$	a_1	b_1	ω_1
48	5.14/9	1.12(7)	0.50(5)	0.02(22)	0.06(1)	0.4(2)	0.4(7)
64	4.47/6	1.1(1)	0.55(8)	0.1(3)	0.05(2)	0.7(5.2)	0.7(3.0)
96	2.92/3	1.15(3)	0.4(1)	0.09(3)	0.09(6)	6.24(1)	1.4(2)
48	8.83/10	1.13(5)	0.608	0.03(18)	0.0390(9)	0.4(2)	0.4(7)
64	5.03/7	1.1(1)	0.608	0.1(4)	0.038(1)	0.4(2.3)	0.5(2.9)
96	4.41/4	1.16(2)	0.608	0.10(2)	0.038(1)	8.900(6)	1.5(2)
48	7.09/10	1.13(5)	0.58	0.03(19)	0.044(1)	0.4(2)	0.4(7)
64	4.62/7	1.1(1)	0.58	0.1(3)	0.043(1)	0.5(3.4)	0.6(3.0)
96	3.98/4	1.16(2)	0.58	0.10(2)	0.043(2)	7.903(7)	1.4(2)

Table IV. Fits of $R_{[10]}$ to Eq. (C1) for the special transition with $b_1 = 0$.

L_{\min}	χ^2/DF	κ_c	y_t	$R_{[10]}^c$	a_1
48	108.12/11	1.25(1)	0.29(5)	0.160(7)	0.15(3)
64	37.02/8	1.206(7)	0.44(8)	0.138(4)	0.08(3)
96	4.41/5	1.184(6)	0.4(1)	0.123(4)	0.10(7)
128	0.33/2	1.175(5)	0.8(3)	0.117(4)	0.01(2)
48	145.25/12	1.206(2)	0.608	0.1398(8)	0.0394(9)
64	41.39/9	1.197(2)	0.608	0.133(1)	0.037(1)
96	6.35/6	1.180(3)	0.608	0.121(2)	0.038(1)
128	0.84/3	1.175(7)	0.608	0.116(5)	0.035(2)
48	138.73/12	1.208(2)	0.58	0.1407(8)	0.045(1)
64	40.01/9	1.198(2)	0.58	0.134(1)	0.042(1)
96	5.84/6	1.181(4)	0.58	0.121(2)	0.043(2)
128	0.98/3	1.175(7)	0.58	0.116(5)	0.040(2)

Table V. Fits of $g(L/2)$ to Eq. (B1) for the large- t side of Kosterlitz-Thouless-like transition at $\kappa = 10$.

t	L_{\min}	χ^2/DF	a	b
0.027	48	208.63/3	1.115(3)	-0.1700(6)
	64	36.28/2	1.080(4)	-0.1628(8)
	96	0.96/1	1.01(1)	-0.150(2)
0.03	48	591.62/3	1.016(2)	-0.1264(4)
	64	127.87/2	0.980(2)	-0.1187(5)
	96	6.02/1	0.929(5)	-0.108(1)
0.035	48	437.57/3	0.990(1)	-0.0979(3)
	64	119.14/2	0.964(2)	-0.0924(4)
	96	5.54/1	0.925(4)	-0.0841(9)
0.04	48	96.45/3	1.010(2)	-0.0881(5)
	64	28.96/2	0.991(3)	-0.0839(7)
	96	0.65/1	0.950(8)	-0.075(2)
0.045	48	24.06/3	1.017(3)	-0.0788(7)
	64	6.70/2	1.003(4)	-0.076(1)
	96	1.05/1	0.97(1)	-0.069(3)
0.05	48	18.18/3	1.017(4)	-0.070(1)
	64	9.31/2	1.004(6)	-0.067(1)
	96	0.98/1	0.96(2)	-0.058(4)

Table VI. Fits of $g(L/2)$ to Eq. (B1) for the ordinary critical phase at $\kappa = 0.4$.

L_{\max}	L_{\min}	χ^2/DF	a	b
192	32	7.02/4	66.6(1.8)	-2.374(7)
	48	4.01/3	76.5(6.5)	-2.41(2)
	64	2.15/2	90.9(14.1)	-2.45(4)
	96	1.41/1	141.2(77.8)	-2.5(1)
128	32	2.62/3	66.2(1.8)	-2.373(7)
	48	0.84/2	73.9(6.4)	-2.40(2)
	64	0.002/1	83.7(13.7)	-2.43(4)

Table VII. Fits of $g(L/2)$ to Eq. (C2) for the extraordinary phase at $\kappa = 2, 3, 5, 7$ and 10.

κ	L_{\min}	χ^2/DF	a	l_0	\hat{q}
2	16	1.93/4	0.68(1)	3.5(3)	0.32(1)
	32	0.12/3	0.76(8)	2.2(9)	0.38(5)
	48	0.07/2	0.7(2)	3.3(4.9)	0.3(2)
	64	0.03/1	0.8(9)	1.7(8.1)	0.4(5)
	16	177.76/5	1.170(2)	0.648(8)	0.59
	32	8.09/4	1.248(7)	0.40(2)	0.59
	48	0.89/3	1.29(2)	0.31(3)	0.59
	64	0.12/2	1.31(4)	0.25(7)	0.59
	96	0.07/1	1.33(8)	0.2(1)	0.59
3	16	2.74/4	1.11(8)	1.0(2)	0.42(3)
	32	1.01/3	0.9(1)	2.3(1.3)	0.33(6)
	48	0.42/2	1.5(2.0)	0.3(1.2)	0.5(5)
	16	16.72/5	1.649(3)	0.257(4)	0.59
	32	7.21/4	1.69(1)	0.21(1)	0.59
	48	0.42/3	1.73(2)	0.16(2)	0.59
	64	0.31/2	1.75(5)	0.15(4)	0.59
	96	0.003/1	1.7(1)	0.2(2)	0.59
5	16	2.17/4	2.7(9)	0.03(3)	0.7(1)
	32	1.30/3	1.5(6)	0.3(5)	0.5(2)
	48	1.14/2	2.7(6.5)	0.02(22)	0.7(8)
	64	0.99/1	1.1(1.3)	1.2(7.4)	0.3(5)
	16	2.57/5	2.221(6)	0.053(1)	0.59
	32	1.72/4	2.20(2)	0.058(5)	0.59
	48	1.15/3	2.23(4)	0.05(1)	0.59
	64	1.08/2	2.21(7)	0.05(2)	0.59
	96	0.85/1	2.3(2)	0.04(4)	0.59
7	16	2.29/4	4.4(2.7)	0.001(4)	0.7(2)
	32	1.34/3	1.7(9)	0.1(3)	0.4(2)
	16	3.31/5	2.692(9)	0.0108(5)	0.59
	32	1.67/4	2.66(3)	0.013(2)	0.59
	48	0.83/3	2.70(5)	0.010(3)	0.59
	64	0.06/2	2.63(9)	0.015(7)	0.59
	96	0.001/1	2.6(2)	0.02(2)	0.59
	10	16	12.53/5	3.35(2)	0.00084(8)
32		0.93/4	3.22(4)	0.0017(4)	0.59
48		0.91/3	3.21(8)	0.0018(7)	0.59
64		0.91/2	3.2(1)	0.002(1)	0.59
96		0.08/1	3.0(3)	0.01(1)	0.59

Table VIII. Fits of the summed scaled stiffness $\sum \rho_s L$ over $\kappa = 2, 3, 5, 7$ and 10 to Eq. (C4) for the extraordinary phase.

L_{\max}	L_{\min}	χ^2/DF	A	B
192	32	95.84/4	0.2(2)	4.47(5)
	48	28.71/3	-2.3(4)	5.10(9)
	64	3.98/2	-5.3(7)	5.8(2)
	96	0.45/1	-8.8(2.0)	6.5(4)
128	32	64.32/3	0.5(2)	4.41(5)
	48	16.33/2	-1.9(4)	5.0(1)
	64	0.77/1	-4.6(8)	5.6(2)